

# Supporting Information for "Increasing methane emissions and widespread cold-season release from high-Arctic regions detected through atmospheric measurements"

Rebecca H. Ward<sup>1</sup>, Colm Sweeney<sup>2</sup>, John B. Miller<sup>2</sup>, Mathias Goeckede<sup>3</sup>,

Tuomas Laurila<sup>4</sup>, Juha Hatakka<sup>4</sup>, Viktor Ivakov<sup>5</sup>, Motoki Sasakawa<sup>6</sup>,

Toshinobu Machida<sup>6</sup>, Shinji Morimoto<sup>7</sup>, Daisuke Goto<sup>8</sup>, Anita L. Ganesan<sup>1</sup>

<sup>1</sup>School of Geographical Sciences, University of Bristol, Bristol, United Kingdom

<sup>2</sup>National Oceanic and Atmospheric Administration/Global Monitoring Laboratory, Boulder, CO 80305

<sup>3</sup>Max Planck Institute for Biogeochemistry, Jena, Germany

<sup>4</sup>Finnish Meteorological Institute, Helsinki, Finland

<sup>5</sup>Voeikov Main Geophysical Observatory, St Petersburg, Russia

<sup>6</sup>Center for Global Environmental Research, National Institute for Environmental Studies, Tsukuba, Ibaraki, Japan

<sup>7</sup>Tohoku University, Sendai, Japan

<sup>8</sup>National Institute of Polar Research, Tokyo, Japan

## Contents of this file

1. Text S1
  2. Figures S1 to S10
  3. Tables S1 to S6
-

## Introduction

This supporting information file includes extra details to describe the method and inputs to the hierarchical Bayesian inversion in Figures S1-S4 and S7 and Tables S1-S4. It also includes a description of the uncertainty analysis across all methods (Text S1). Further details on inversion outputs are given, including sensitivity tests (Fig S5-9), inversion performance (Fig S8-9), posterior emissions maps (Fig S10) and total emissions for each region (Table S5). Table S6 shows the percentage of land type and lake class coverage using the BAWLD (Olefeldt et al., 2021) dataset.

**Text S1.**

Uncertainties for the mole fraction enhancements trend and temperature anomaly trend were calculated using a method designed in Sweeney et al., 2016 (Sweeney et al., 2016) and replicated to the best of our ability for this work. Uncertainties in the enhancements were calculated using a non-parametric bootstrapping technique. This was done by fitting a Gaussian kernel distribution, a non-parameteric distribution, to the de-trended enhancement data points across all years, then 1000 times, sampling from the distribution to add a random offset to each data point in the time series, and fitting a slope to each of those means. Enhancement and temperature anomaly trend errors quoted are the standard deviation of these 1000 slopes to give a  $1\sigma$  error in the trend.

A similar sampling method was used for the emissions trend, derived from the inversions. One thousand slopes were found from re-sampling a normal distribution around each monthly emission estimate, whereby the standard deviation of each point is calculated from 95% confidence intervals derived from 250000 iterations of the MCMC trace. Inversion trend errors quoted are twice the standard deviation of these 1000 slopes to give a  $1\sigma$  error in the trend. Errors in the averages were assumed to be fully correlated and quoted to  $1\sigma$ . We used the Python Uncertainties package to calculate correlated uncertainties.

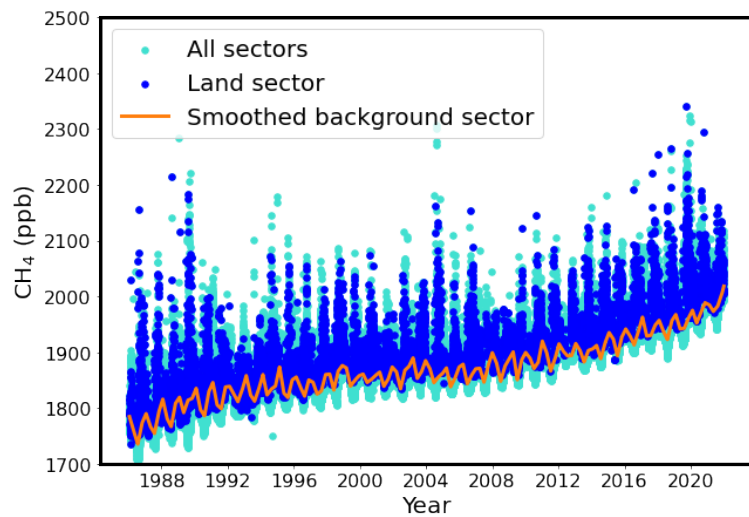


**Figure S1.** Utqiagvik (BRW) measurements showing all data points (light blue), those from the land-sector (dark blue) and the smoothed background (orange line).

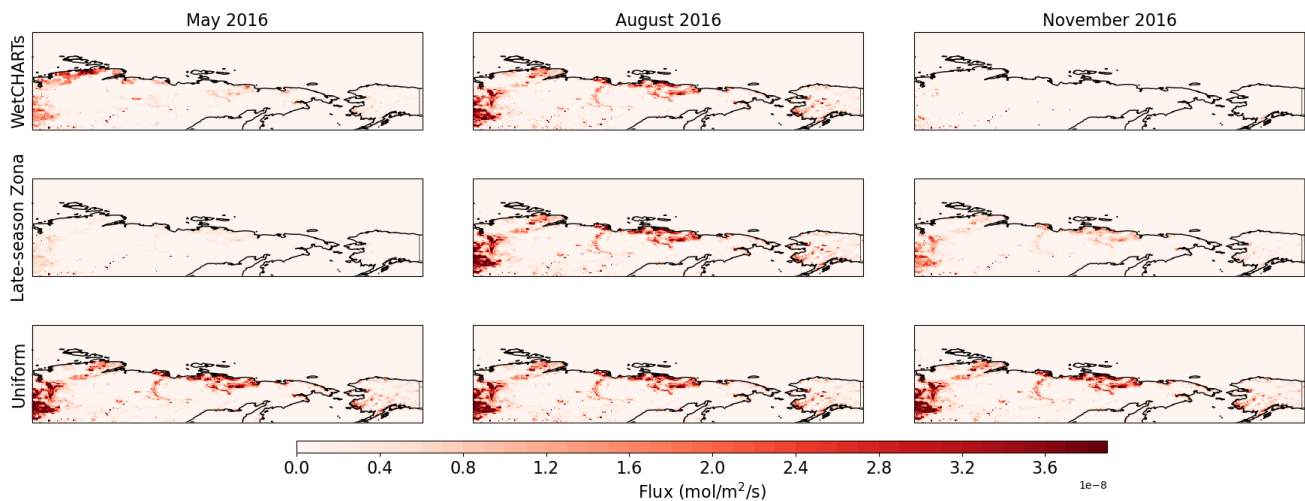


**Figure S2.** Prior emissions maps used in this study for May, August and November with 2016 as an example.

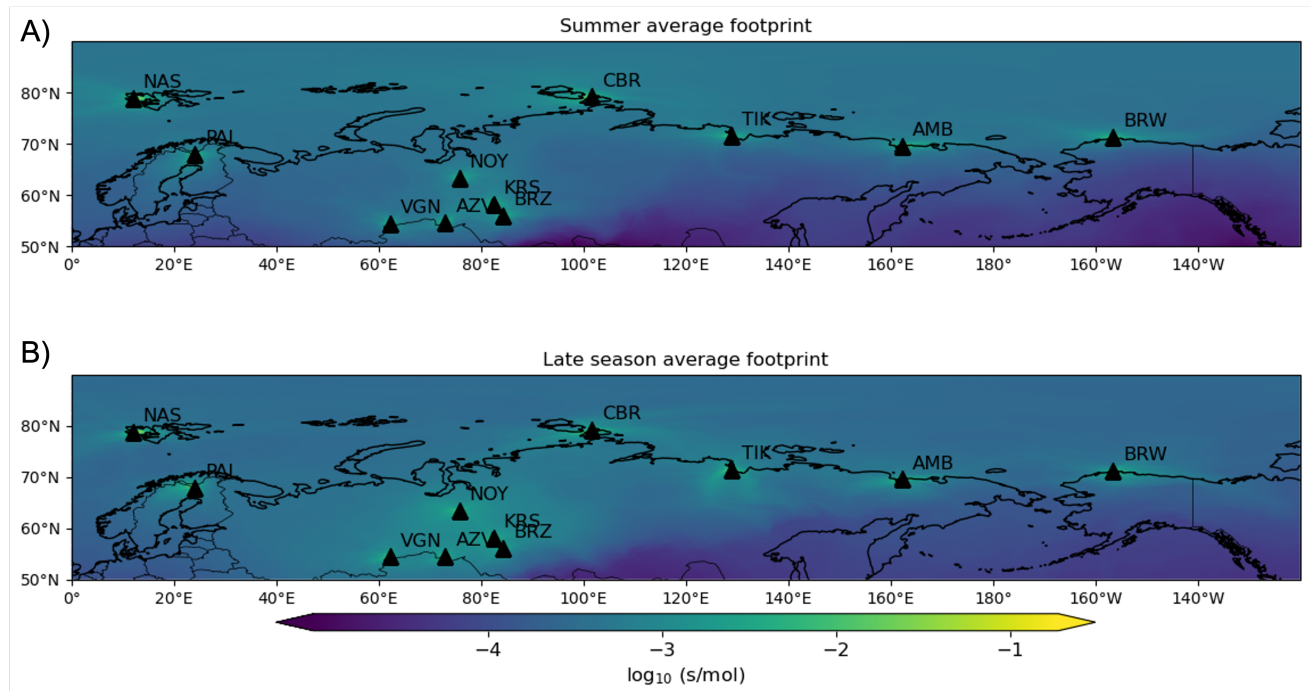


**Figure S3.** Average footprint maps for all sites for A) the summertime months, and B) the late season months .

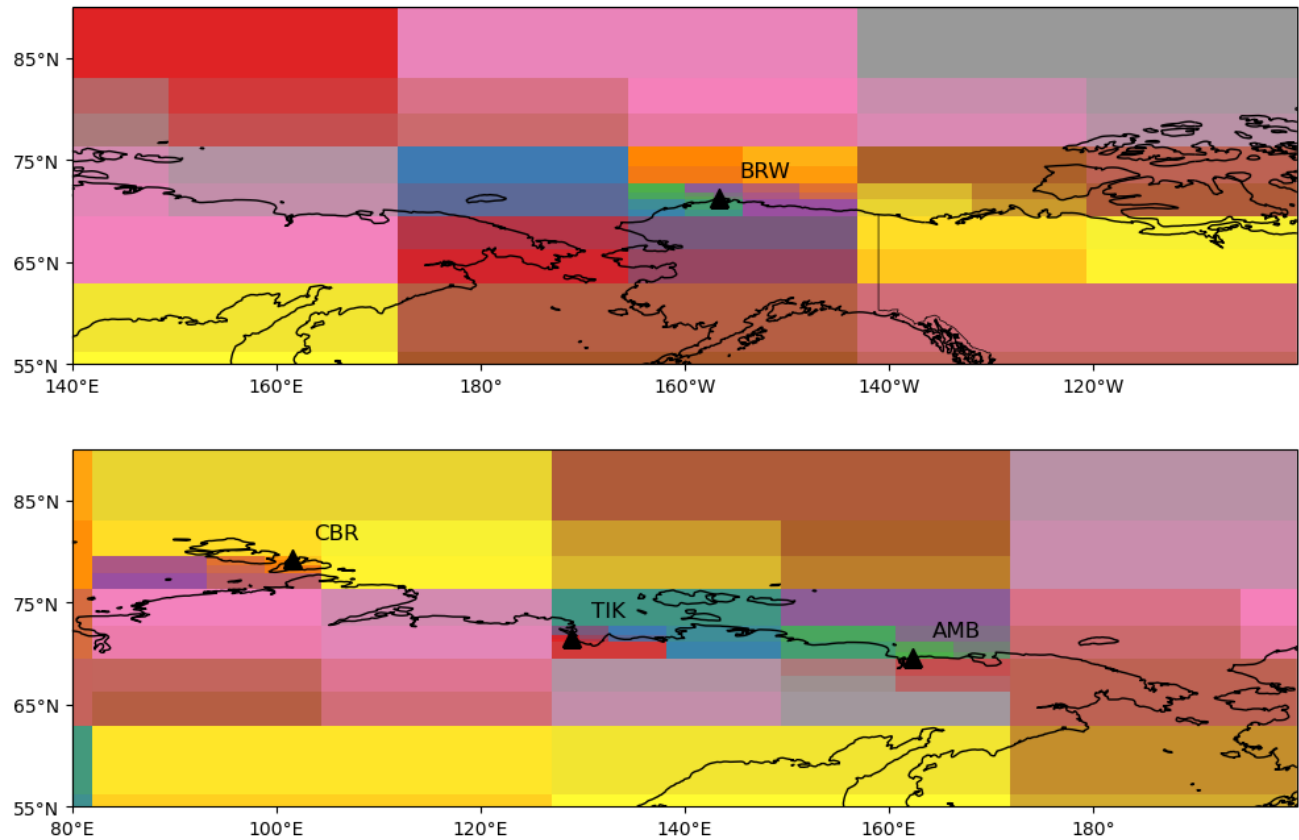


**Figure S4.** Inversion basis functions used in A) the BRW inversion and B) the Siberia inversion.

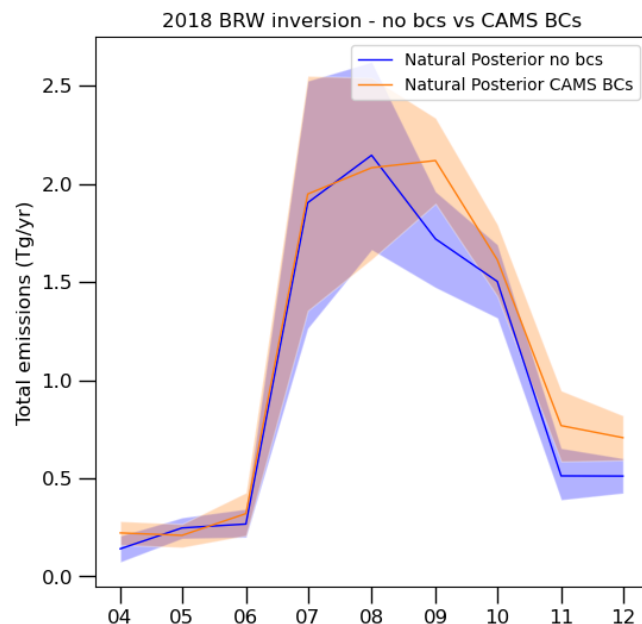


**Figure S5.** Emissions from natural sources on the land over the North Slope of Alaska for the period Apr 2018 to Dec 2018. For the inversion where the wind-sector background is subtracted from the data (blue) and for the inversion that uses CAMS fields for the southern boundary (orange).

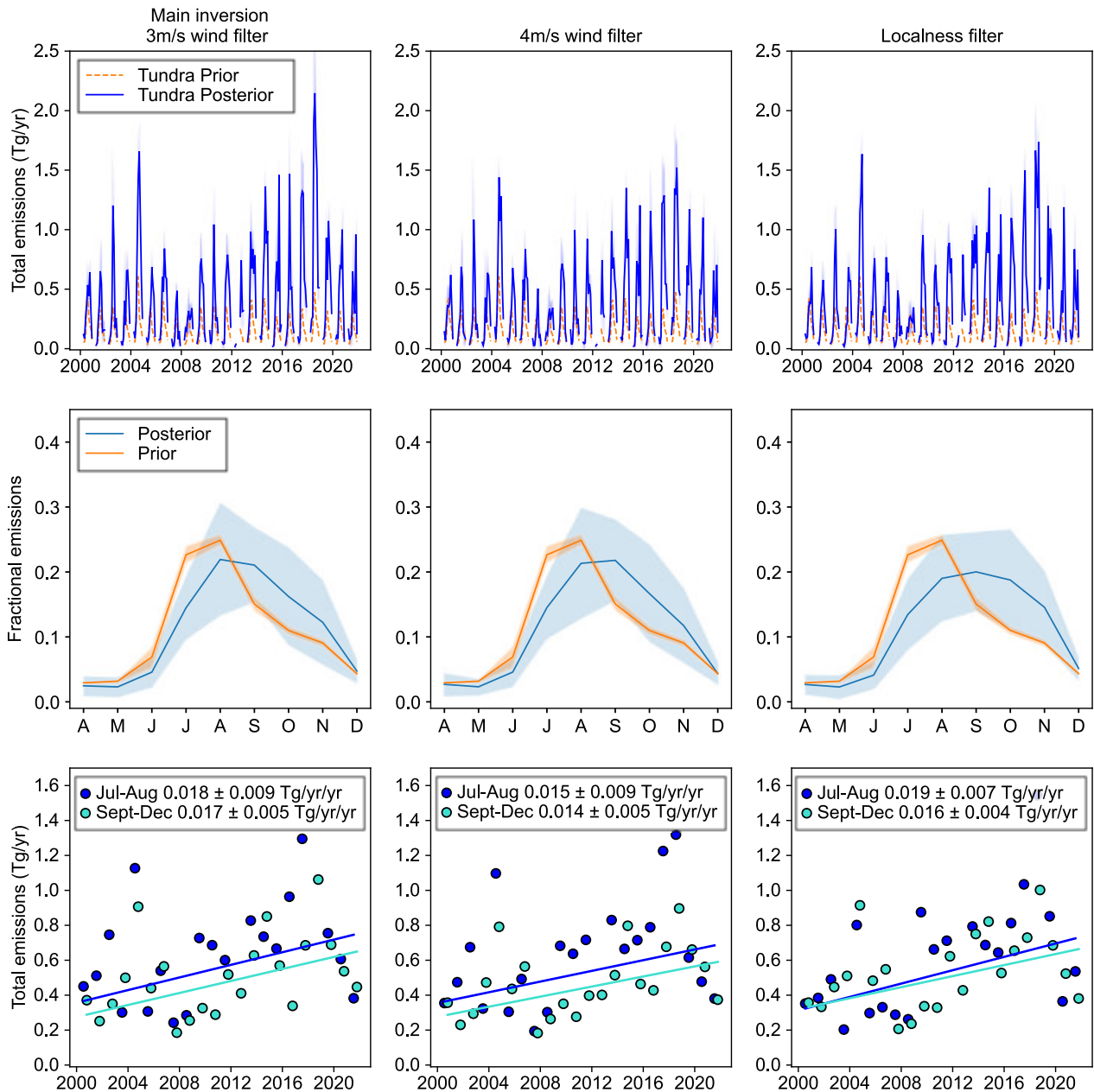


**Figure S6.** Main result for the Late season Zona prior (first column) compared to two sensitivity tests for the BRW inversion (second two columns). The first test increases the wind speed filter from 3m/s to 4m/s, the second uses a localness filter. Both cases are used to assess whether the main inversion suitably accounts for local emissions around the site. Top row: comparison of total emissions for each test. Middle row: comparison of seasonal profile. Bottom row: comparison of emissions trend.

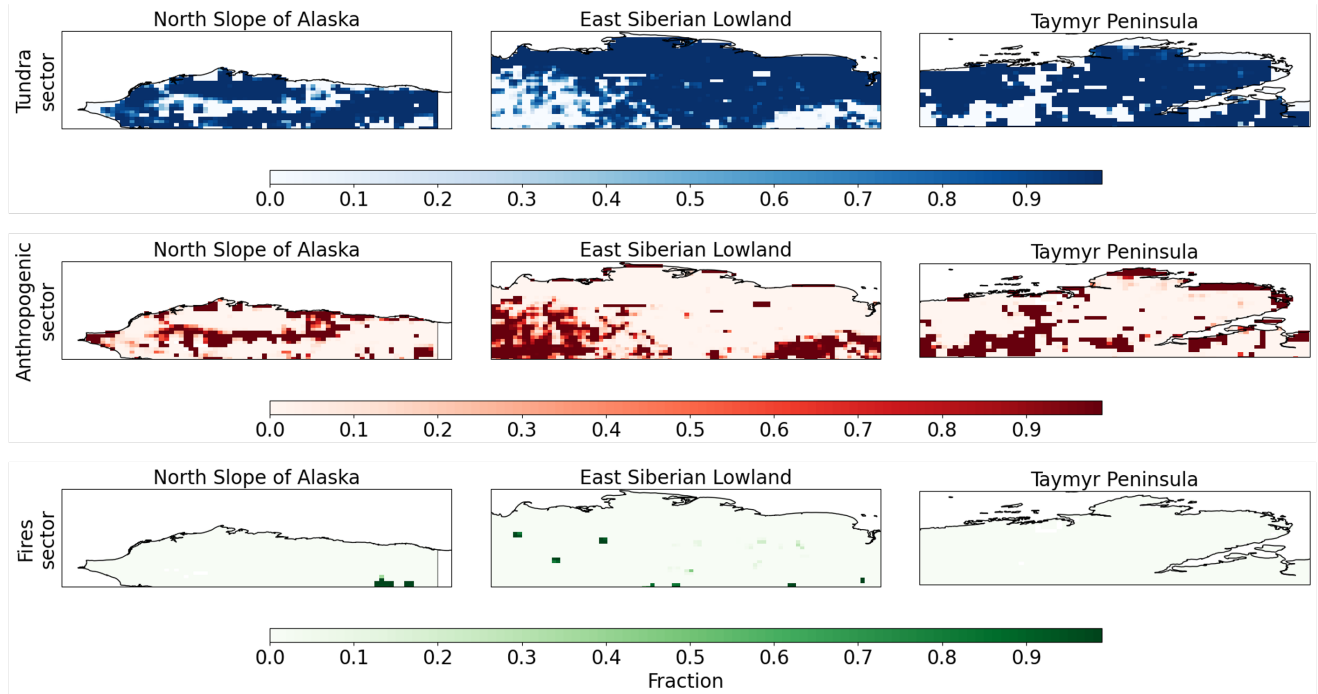


**Figure S7.** The fraction of sector emissions in each grid cell, shown here for June 2015.

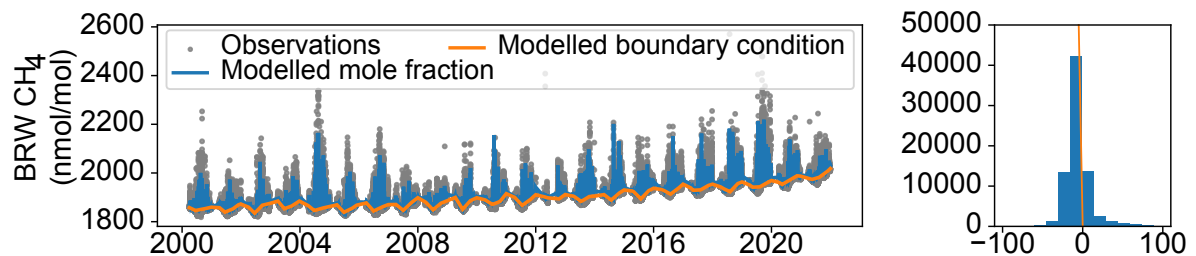


**Figure S8.** Inversion performance for the BRW inversions. Left: Modelled mole fractions and boundary conditions for BRW compared to observations. The background for BRW is the smoothed background derived in the wind sector method. Right: Histograms of the difference between modelled and observed mole fractions.

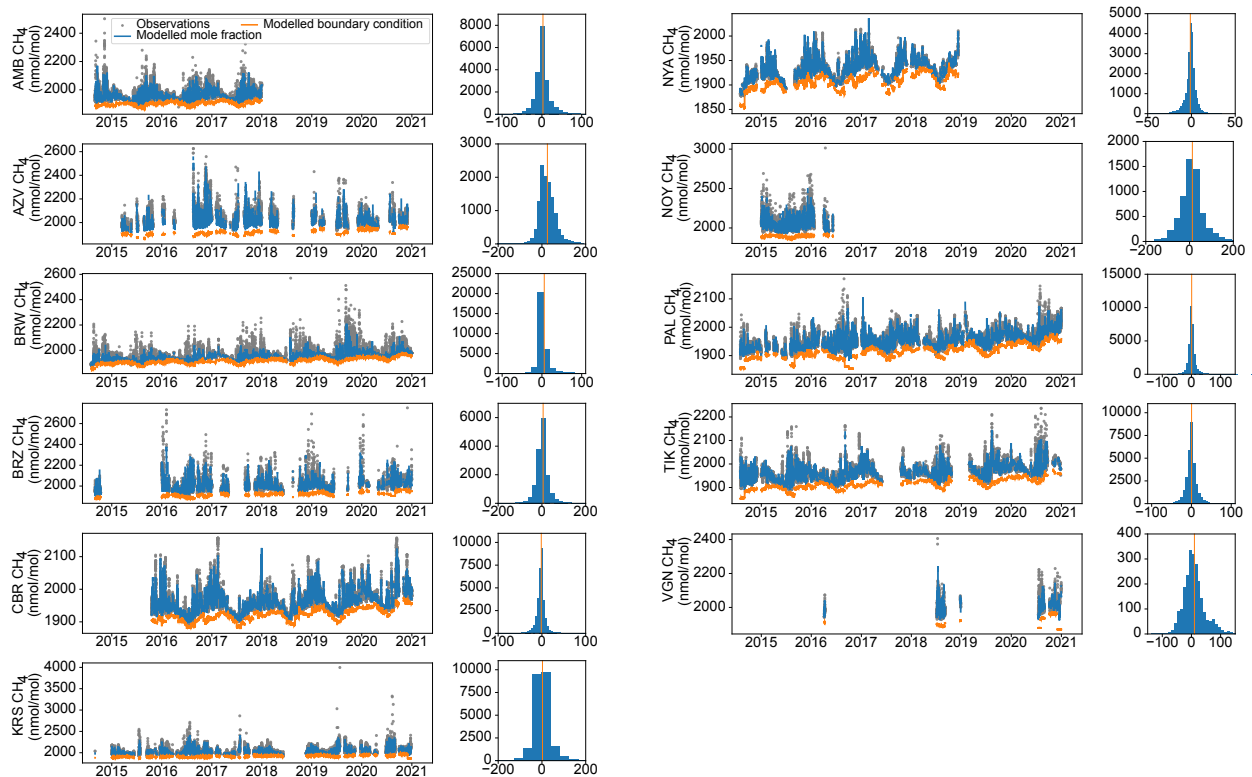


**Figure S9.** Inversion performance for the Siberia inversions. Left: Modelled mole fractions and boundary conditions for each site, compared to modelled observations. Right: Histograms of the difference between modelled and observed mole fractions.

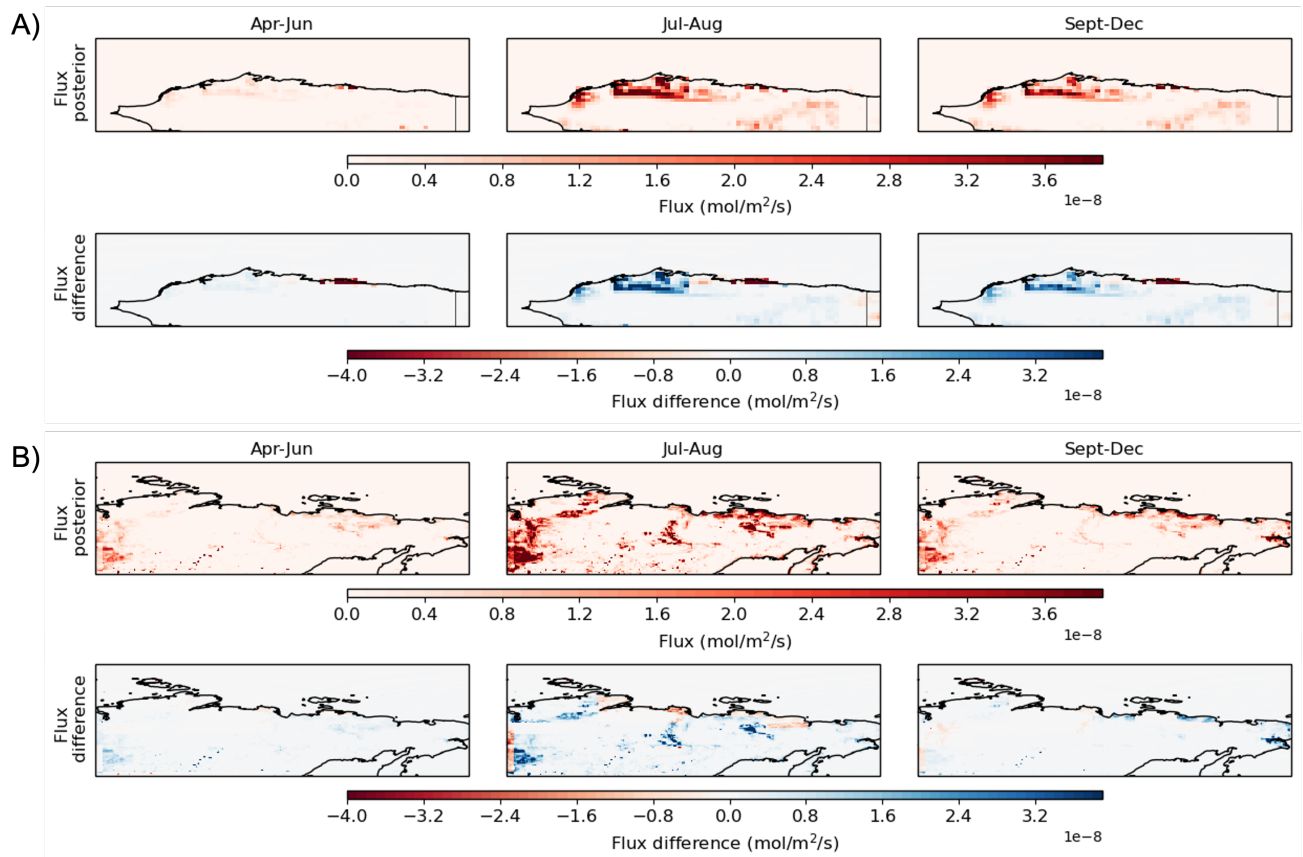


**Figure S10.** Average posterior emissions and the difference between posterior and Late-season Zona prior emissions (prior subtracted from posterior) for the early, summertime and late seasons for A) the North Slope of Alaska and B) Siberia (covering the Taymyr Peninsula and East Siberian Lowlands).

**Table S1.** Measurement stations and years used in this study.

<b>Site</b>	<b>Network</b>	<b>Lat,Lon</b>	<b>Dates used</b>	<b>Inlet height</b>	<b>Reference</b>
Ambarchik, Russia	MPI-BGC	69.62°N, 162.3°E	2015-2017	20 (mag)	(Göckede et al., 2023)
Azovo, Russia	JR-STATION	54.71°N, 73.03°E	2015-2020	50	(Sasakawa, 2023a)
Barrow, Alaska	NOAA	71.32°N, 23.39°W	1986-2021	16	(Schuldt et al., 2023)
Berezorechka, Russia	JR-STATION	56.14°N, 84.33°E	2015-2020	80	(Sasakawa, 2023b)
Cape Bara- nova, Russia	FMI	79.16°N, 101.75°E	2015-2020	10	(Laurila, 2023).
Karaevoe, Russia	JR-STATION	58.25°N, 82.42°E	2015-2020	67	(Sasakawa, 2023c)
Noyabrsk, Russia	JR-STATION	63.43°N, 75.78°E	2015-2020	43	(Sasakawa, 2023d)
Ny-Alesund, Svalbard	Tohoku University	78.92°N, 11.93°E	2015-2020	10	(Morimoto & Goto, 2019)
Pallas, Fin- land	FMI	67.97°N, 24.12°E	2015-2020	10	(Hatakka & ICOS RI, 2022)
Tiksi, Russia	FMI	71.60°N, 128.89°E	2010-2020	8	(Ivakov et al., 2019)
Vaganovo, Russia	JR-STATION	54.49°N, 62.32°E	2015-2020	85	(Sasakawa, 2023e)

**Table S2.** Emission fields that comprised the priors used in this study. As our inversions run from 2000-2021, where applicable, the years that do not have dataset coverage use the closest available year. Details of how the different wetland priors are created are found in Table S3.

Sector	Source	Resolution	Time period
Wetland emissions	SWAMPs	Monthly	2000-2019
	WetCHARTs	Monthly	2001-2019
	Zona	Monthly	2012-2014
Anthropogenic emissions	EDGAR v5	Annual	2000-2015
Biomass burning emissions	GFED v4	Monthly	2000-2015

**Table S3.** Description of wetland emissions for each prior type.

Prior name	Spatial distribution	Seasonal profile	Scaling factor
WetCHARTs	SWAMPs (monthly and IAV)	WetCHARTs (monthly and IAV)	46 Tg/yr(Saunois et al., 2020). Global Methane Budget value for top-down 30 - 90°N emissions from wetland sources.
Late-season Zona	SWAMPs July distribution of each seasonal year for each month	Zona et al., 2016 profile (Zona et al., 2016) (same for each year)	46 Tg/yr(Saunois et al., 2020)
Uniform	SWAMPs July distribution for each month	WetCHARTs July value for every month	46 Tg/yr(Saunois et al., 2020)

**Table S4.** Region latitude/longitude bounds and total area.

<b>Region</b>	<b>Latitude bounds</b>	<b>Longitude bounds</b>	<b>Area (m<sup>2</sup>)</b>
North Slope	67.03 - 71.25	193.89 - 218.86	3.70 x 10 <sup>11</sup>
East Siberian Lowlands	64.92 - 72.89	129.91 - 161.90	9.95 x 10 <sup>11</sup>
Taymyr Peninsula	71.95 - 77.58	89.83 - 114.80	3.67 x 10 <sup>11</sup>

**Table S5.** Total emissions from each region for each time period in Tg/yr and by area in  $\mu\text{g}/\text{m}^2/\text{s}$ .

Region		Annual	Early-season	Summertime	Late-season
North Slope of Alaska	Total (Tg/yr)	0.42	0.10	0.70	0.51
	By area ( $\mu\text{g}/\text{m}^2/\text{s}$ )	0.04	0.03	0.36	0.13
East Siberian Lowlands	Total (Tg/yr)	2.39	1.12	5.65	2.51
	By area ( $\mu\text{g}/\text{m}^2/\text{s}$ )	0.08	0.16	1.08	0.24
Taymyr Peninsula	Total (Tg/yr)	0.47	0.12	1.00	0.63
	By area ( $\mu\text{g}/\text{m}^2/\text{s}$ )	0.04	0.04	0.52	0.16

**Table S6.** Percentage land type and lake class coverage of each region. Found using the Boreal-Arctic Wetland and Lake Dataset fractional land cover estimates (Olefeldt et al., 2021).

		Percentage coverage (%)		
Land Type		North Slope of Alaska	East Siberian Lowland	Taymyr Peninsula
	Glaciers and permanent snow	0.1	0.0	0.0
	Rocklands	17.7	7.3	10.0
	Dry tundra	63.0	43.6	69.7
	Boreal forest	5.4	29.9	0.0
Wetlands	All wetland types	9.0	11.6	14.3
	Permafrost bog	3.8	4.5	8.9
	Wetland tundra	5.0	6.9	5.4
	Marsh	0.1	0.1	0.0
	Bog	0.0	0.0	0.0
	Fen	0.0	0.0	0.0
Lakes	All lakes	4.4	6.9	5.3
	Large lakes	0.7	1.8	2.0
	Mid -sized peatland lakes	1.3	1.0	0.4
	Mid sized yedoma lakes	0.3	1.9	0.5
	Mid sized glacial lakes	1.2	0.9	0.9
	Small peatland lakes	0.4	0.4	0.5
	Small yedoma lakes	0.2	0.7	0.6
	Small glacial lakes	0.3	0.2	0.4

## References

- Göckede, M., Reum, F., & Heimann, M. (2023). *Atmospheric mixing ratios of CO<sub>2</sub> and CH<sub>4</sub> at Ambarchik, NE Siberia, 2014-2017 [Dataset]*. Retrieved from <https://doi.org/10.17617/3.1STIJV>
- Hatakka, J., & ICOS RI. (2022). *ICOS Atmosphere Level 2 data, Pallas, release 2022-1 [Dataset]*. ICOS ERIC – Carbon Portal. Retrieved from <https://meta.icos-cp.eu/collections/6NpfwCwt7VJxybU-USxxpUmC>
- Ivakov, V., Laurila, T., Dlugokencky, E., & Hatakka, J. (2019). *Atmospheric CH<sub>4</sub> at Tiksi by Finnish Meteorological Institute, dataset published as CH<sub>4</sub>\_tik\_surface-insitu\_fmi\_data1 at WDCGG, ver. 2022-07-08-2150 [Dataset]*. World Data Centre for Greenhouse Gases. Retrieved from <https://gaw.kishou.go.jp/> doi: 10.50849/WDCGG\_0025-2002-1002-01-01-9999
- Laurila, T. (2023). *Data on atmospheric concentrations of CH<sub>4</sub>, CO and meteorological parameters at Baranova site, Russia [Dataset]*. Finnish Meteorological Institute. Retrieved from <https://fmi.b2share.csc.fi/records/cd485d0c767d47d6b0028c73620eca38>
- Morimoto, S., & Goto, D. (2019). *CH<sub>4</sub> concentrations observed at Ny-Alesund, Svalbard [Dataset]*. Tohoku University and National Institute of Polar Research. Retrieved from [https://polaris.nipr.ac.jp/~parc/pub/v041/nipr\\_parc\\_122\\_0004.txt](https://polaris.nipr.ac.jp/~parc/pub/v041/nipr_parc_122_0004.txt)
- Olefeldt, D., Hovemyr, M., Kuhn, M. A., Bastviken, D., Bohn, T. J., Connolly, J., ... Watts, J. D. (2021, May). The Boreal-Arctic Wetland and Lake Dataset (BAWLD). *Earth System Science Data Discussions*, 1–40. doi: 10.5194/essd-2021-140
- Sasakawa, M. (2023a). *Semi-continuous observational data for atmospheric CO<sub>2</sub> and CH<sub>4</sub> mixing ratios at Azovo, ver1.0 [Dataset]*. Earth System Division, NIES. Retrieved from

- <https://www.nies.go.jp/doi/10.17595/20231117.007-e.html>
- Sasakawa, M. (2023b). *Semi-continuous observational data for atmospheric CO<sub>2</sub> and CH<sub>4</sub> mixing ratios at Berezorechka, ver1.0 [Dataset]*. Earth System Division, NIES. Retrieved from <https://www.nies.go.jp/doi/10.17595/20231117.001-e.html>
- Sasakawa, M. (2023c). *Semi-continuous observational data for atmospheric CO<sub>2</sub> and CH<sub>4</sub> mixing ratios at Karasevoe, ver1.0 [Dataset]*. Earth System Division, NIES. Retrieved from <https://www.nies.go.jp/doi/10.17595/20231117.002-e.html>
- Sasakawa, M. (2023d). *Semi-continuous observational data for atmospheric CO<sub>2</sub> and CH<sub>4</sub> mixing ratios at Noyabrsk, ver1.0 [Dataset]*. Earth System Division, NIES. Retrieved from <https://www.nies.go.jp/doi/10.17595/20231117.004-e.html>
- Sasakawa, M. (2023e). *Semi-continuous observational data for atmospheric CO<sub>2</sub> and CH<sub>4</sub> mixing ratios at Vaganovo, ver1.0 [Dataset]*. Earth System Division, NIES. Retrieved from <https://www.nies.go.jp/doi/10.17595/20231117.008-e.html>
- Saunois, M., Stavert, A. R., Poulter, B., Bousquet, P., Canadell, J. G., Jackson, R. B., ... Zhuang, Q. (2020, July). The Global Methane Budget 2000–2017. *Earth System Science Data*, 12(3), 1561–1623. doi: <https://doi.org/10.5194/essd-12-1561-2020>
- Schuldt, K. N., Mund, J., Aalto, T., Arlyn Andrews, Apadula, F., Jgor Arduini, ... Mirosław Zimnoch (2023). *Multi-laboratory compilation of atmospheric carbon dioxide data for the period 1983–2022; obspack\_ch4\_1\_globalviewplus\_v6.0\_2023-12-01 [Dataset]*. NOAA Global Monitoring Laboratory. Retrieved from [https://gml.noaa.gov/ccgg/obspack/data.php?id=obspack\\_ch4\\_1\\_GLOBALVIEWplus\\_v6.0\\_2023-12-01](https://gml.noaa.gov/ccgg/obspack/data.php?id=obspack_ch4_1_GLOBALVIEWplus_v6.0_2023-12-01)
- Sweeney, C., Dlugokencky, E., Miller, C. E., Wofsy, S., Karion, A., Dinardo, S., ... Tans, P. (2016). No significant increase in long-term CH<sub>4</sub> emissions on North Slope of Alaska despite

significant increase in air temperature. *Geophysical Research Letters*, 43(12), 6604–6611.

doi: <https://doi.org/10.1002/2016GL069292>

Zona, D., Gioli, B., Commane, R., Lindaas, J., Wofsy, S. C., Miller, C. E., ... Oechel, W. C. (2016, January). Cold season emissions dominate the Arctic tundra methane budget. *Proceedings of the National Academy of Sciences*, 113(1), 40–45. doi: 10.1073/pnas.1516017113